

Absolute Proper motions Outside the Plane(APOP) A step towards the GSC2.4

Zhaoxiang Qi¹, Yong Yu¹, Beatrice Bucciarelli², Mario G. Lattanzi², Richard L. Smart², Alessandro Spagna², Brian J. McLean³, Zhenghong Tang¹, Hugh R.A. Jones⁴, Roberto Morbidelli², Luciano Nicastro⁵, Alberto Vecchiato²

ABSTRACT

We present a new catalog of absolute proper motions and updated positions derived from the same Space Telescope Science Institute digitized Schmidt survey plates utilized for the construction of the Guide Star Catalog II. As special attention was devoted to the absolutization process and removal of position, magnitude and color dependent systematic errors through the use of both stars and galaxies, this release is solely based on plate data outside the galactic plane, i.e. $|b| \geq 27^\circ$. The resulting global zero point error is less than 0.6 mas/yr, and the precision better than 4.0 mas/yr for objects brighter than $R_F = 18.5$, rising to 9.0 mas/yr for objects with magnitude in the range $18.5 < R_F < 20.0$. The catalog covers 22,525 square degrees and lists 100,777,385 objects to the limiting magnitude of $R_F \sim 20.8$. Alignment with the International Celestial Reference System (ICRS) was made using 1288 objects common to the second realization of the International Celestial Reference Frame (ICRF2) at radio wavelengths. As a result, the coordinate axes realized by our astrometric data are believed to be aligned with the extragalactic radio frame to within ± 0.2 mas at the reference epoch J2000.0. This makes our compilation one of the deepest and densest ICRF-registered astrometric catalogs outside the galactic plane. Although the Gaia mission is poised to set the new standard in catalog astronomy and will in many ways supersede this catalog, the methods and procedures reported here will prove useful to remove astrometric magnitude- and color-dependent systematic errors from the next generation of ground-based surveys reaching significantly deeper than the Gaia catalog.

Subject headings: astrometry – catalogs – absolute proper motions–classification– reference systems– astronomical data bases: miscellaneous

1. INTRODUCTION

The Second Generation Guide Star Catalogue, or GSC-II, is an all-sky catalog of objects built from the uncompressed Digitized Sky Surveys that the Space Telescope Science Institute (STScI) created from the Palomar and UK Schmidt survey

plates (GSC2.3, Lasker et al. 2008). The GSC-II was primarily created to continue providing guide star information¹ and observation planning support, including protection from nearby bright objects to the new generation ultra-sensitive cameras installed on the Hubble Space Telescope (HST) since the first GSC. Thanks to its relatively faint magnitude limit and multi-band photometry, GSC-II is also employed at some of the largest ground-based facilities such as GEMINI, VLT and LAMOST. In the most recent version (GSC2.3.4 in HST operations), it was found that

¹Shanghai Astronomical Observatory, Chinese Academy of Sciences, 80 Nandan Road, 200030 Shanghai, China.

²INAF–Osservatorio Astrofisico di Torino, Strada Osservatorio 20, 10025 Pino Torinese, TO, Italy.

³Space Telescope Science Institute, 3700 San Martin Drive, Baltimore, MD 21218, USA.

⁴Centre for Astrophysics Research, University of Hertfordshire, Hatfield AL10 9AB, UK.

⁵INAF–IASF, Bologna, Italy.

¹In this respect, GSC-II includes the first generation GSC, or GSC-I (Lasker et al. 1990).

the derived proper motions, although compliant with the Hubble operations, suffered from significant systematic errors, especially in the southern hemisphere, and for this reason they were not included in the version released to the astronomical community. This limited the scientific and also technical (e.g., accurate operation of multi-fiber spectrographs) usefulness of the public GSC2.3; various experiments were then initiated to investigate on the sources of such systematic errors and to explore alternative methods for improving the proper motion accuracy (Spagna et al. 2004; Tang et al. 2008). Astrophysically, large samples of accurate absolute proper motions to faint magnitudes are fundamental observables in Milky Way studies to gain, e.g., further insight into the recently discovered evidence of unexpected chemokinematical features (Spagna et al. 2010). These new findings bear the potential to shed new light on the origin and evolution of our Galaxy (Curir et al. 2014, 2012), and ultimately on its role in cosmology (Lattanzi 2012).

In this paper we concentrate on the recalibration of the GSC-II proper motions; however, we also discuss the catalog release (which includes a recalibration of the positions); the catalog, in the form presented here, will be made available at Strasbourg astronomical Data Center (CDS) with the publication of this article.

Assuming we can consider the proper motions of galaxies to be zero, there are two ways to exploit this in the determination of absolute proper motions:

- One is the *direct* way; here, all the observations obtained at different epochs are directly transformed into one system using galaxies as reference objects; therefore, absolute proper motions are a natural derivation within this approach.
- The other possibility is to bring all the observations into a common system using stars (instead of galaxies) as reference objects from which to calculate relative proper motions of all of the measured objects. Then, render those proper motions absolute by subtracting the pseudo proper motions of the galaxies.

The GSC-II object classification is based on

star/non-star criteria rather than star/galaxy. This was done for operational reasons in order to prioritize reliability of the star classification at the cost of a less accurate, more generic, non-star classification. Therefore, non-stars will be a mix of blended objects, faint stars and galaxies, providing a heterogeneous reference system. This mixing is not easy to disentangle, leading to imprecise astrometric transformations; furthermore, the individual accuracy of the measured positions for the non-stars is generally worse than that for stars. Therefore, after a number of dedicated evaluation tests, we decided to adopt the second procedure.

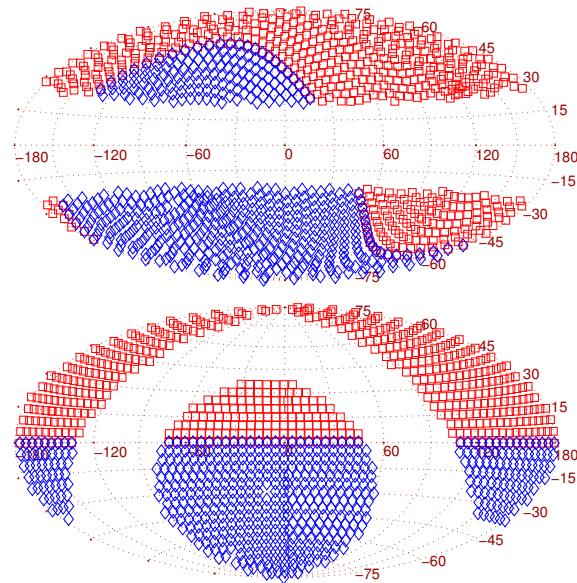


Fig. 1.— The sky distribution of the Schmidt plates used in the APOP catalog. There are 4239 plates used in the reductions. The total area covered by this catalog is $22,525 \text{ deg}^2$. The top figure represents the celestial sphere in Galactic coordinates and the bottom is its analogue in Equatorial coordinates. The blue diamonds represent plates with $\delta < 0^\circ$ and the red squares those with $\delta \geq 0^\circ$.

Due to increasing interstellar extinction as we approach the galactic plane, the number of observable (genuine) galaxies drops to zero. In the end, our reductions only addressed the parts of the celestial sphere with galactic latitudes $|b| \geq 27^\circ$, see Fig. 1. This is only an operational definition of off-the-galactic-plane regions, and clearly depends

on the lack of non-stars for our reductions below that latitude.

The next section describes the plate data used to derive the proper motions in our catalog, which we decided to call “Absolute Proper motions Outside the Plane” or APOP for brevity.

In the 3rd section we present the calibration pipeline and the details of the detection and removal of systematic errors that are dependent on plate position, magnitude and color (hereafter PdE, MdE and CdE, respectively).

In section 4, the anticipated precision is estimated theoretically, and both internal and external precisions are assessed. This section also describes the APOP available to the community through the CDS center in Strasbourg. Finally, the last section presents some conclusions and briefly discusses future plans.

2. PLATE DATA

The observational data come from the STScI Catalogue of Objects and Measured Parameters from All-Sky Surveys (COMPASS) archive of the GSC-II project. This object-oriented database is the repository of the original (raw) measurements (astrometric and photometric) of all of the objects detected on any of the 7000+ survey plates digitized; it also contains the entire set of parameters resulting from all of the plate-based calibrations (astrometry, photometry, and image classification). The details on COMPASS and on the methods used for the derivation of the plate-based quantities can be found in Lasker, Lattanzi, Mc Lean et al. (2008). An important detail worth recalling here is that cross-identification of the same objects detected on different plates was made using a matching radius of 4 arcsec.

The digitized resolution of most plates is 15 $\mu\text{m}/\text{pixel}$ (1 arcsec/pixel), while some plates were scanned at 25 $\mu\text{m}/\text{pixel}$ (1.7 arcsec/pixel, see table 1 of Lasker et al. (2008)). The average accuracy of the measured coordinates is about 0.12-0.13 pixel at intermediate magnitudes (Spagna et al. 1996); also, the average photometric accuracy is about 0.13-0.22 mag, and reliability of the star classification nears 90% (Lasker et al. 2008).

As already stated, the classification is limited to star/non-star, with no galaxy class, which complicates the calculation of absolute proper motions.

For this reason, a new procedure was developed to iteratively refine the selection of genuine galaxies from the non-star objects, as detailed in the next section.

3. CATALOG CONSTRUCTION

There are three critical factors affecting errors of absolute proper motions: a) epoch range spanned by the survey plates employed, b) quality (e.g., intrinsic noise) of the emulsions of that same photographic material along with that of the measuring machines utilized for the digitization process, and 3) modeling the transformation of plates of different epochs to a common reference frame. The third element is really the only one we can work on to improve the calibrations and hopefully derive better proper motions.

It is well known that because of the combined influence of the atmosphere (differential refraction, dispersion, extinction etc.), telescope (guiding errors, distortion of field of view, etc.), photographic plates (uneven response to bending stress, size and distribution of emulsion, low quantum efficiency etc.), and plate scanner (digitizing errors), individual plate coordinates of the detected objects, as well as their magnitudes and colors, can have varied systematic errors that are dependent on position, magnitude and color of the same objects, and these systematics can be different for the different survey plates (see for example Taff et al. 1990; Morrison et al. 1998; Evans & Irwin 1995; Kuimov et al. 2000,).

As proper motions are derived from positions at different epochs, it is likely they will suffer from similar systematic errors. On the other hand, actual (physical) proper motions are expected to exhibit correlations with sky direction, magnitude and color due to the motions of the different stellar populations within the Milky Way. Therefore, one aspect that must be carefully considered when attempting the elimination of the systematic errors mentioned above is not to bias the proper motions with unphysical sources.

Below, we describe both the reduction procedures and assumptions adopted.

3.1. Principles of calibration

We work under the hypothesis that: i) objects (stars and galaxies) physically close on a photographic plate and with similar magnitudes/colors have similar systematic errors, and ii) the absolute proper motions of galaxies are always zero, i.e., they do not depend on their plate position, magnitude or color.

Based on these assumptions, and considering the available plate data, the adopted procedure is to choose a good quality plate as the reference plate and use the objects classed as stars with good image quality² to transform the relevant program plates to the reference plate system.

The major plate-based calibration steps are:

- Remove the PdE with a moving-mean filter³ using stellar objects with good image quality;
- Select galaxies from non-stars via their pseudo (common) motion relative to the reference stars;
- Calibrate the MdE, CdE and the residual PdE of all objects with reference to the galaxies.

Finally, absolute proper motions are calculated from all of the detections at the different plate epochs.

The relevant equations are described below.

For each object, the difference of positions between the reference(plate 1) and one of the corresponding program plates (plate 2) is modeled as:

$$\Delta x_s = x_1 - x_2 = \mu_x \Delta t + D(x_2, y_2) + E(m_2, c_2, x_2, y_2) \quad (1)$$

$$\Delta x_g = D(x_2, y_2) + E(m_2, c_2, x_2, y_2) \quad (2)$$

where $\Delta x_s, \Delta x_g$ represent the individual positional difference of stars and galaxies respectively, and μ_x is a star's absolute proper motion in the reference plate coordinate system; also, Δt is the epoch interval between the reference and program plates, D is the PdE, and E is the combined MdE

²A precise operational definition of good image quality is given in subsection 3.3.

³This moving filter, or moving sub-plate method as it is called in this article, is described in subsection 3.3.

and CdE. Similar equations hold for the y coordinate.

The absolute proper motion μ_x of each star can be separated into the average proper motions $\bar{\mu}_x$ for all reference stars on the plate and a remaining individual proper motion, relative to the reference stars, $d\mu_x$, i.e.

$$\mu_x = \bar{\mu}_x + d\mu_x \quad (3)$$

Removing the systematic error D, beside removing the average MdE and CdE of the reference stars, also removes their average proper motions $\bar{\mu}_x$, while the galaxies will attain a ‘pseudo’ proper motion $-\bar{\mu}_x$.

After this step, the position differences $\Delta x'_s, \Delta x'_g$ of stars and galaxies between the reference and program plates can be expressed as:

$$\begin{aligned} \Delta x'_s &= x_1 - x'_2 = \Delta x_s - (D + \bar{\mu}_x \Delta t) \\ &= d\mu_x \Delta t + E \end{aligned} \quad (4)$$

$$\Delta x'_g = \Delta x_g - (D + \bar{\mu}_x \Delta t) = -\bar{\mu}_x \Delta t + E \quad (5)$$

Equation (5) has a special role in our reduction procedure; for, we iterate exactly on this equation to reject non-stars that are not genuine galaxies. In practice, assuming that all real galaxies will show the common pseudo proper motion $-\bar{\mu}_x$ discussed before, we flag as outliers, i.e. probable blended objects, those that do not⁴. In the end, the selected true galaxies constrain the average proper motions, and MdE and CdE terms. After this stage, the updated position differences $\Delta x''_s, \Delta x''_g$ can be expressed as:

$$\begin{aligned} \Delta x''_s &= x_1 - x''_2 = \Delta' x_s - \Delta' x_g \\ &= d\mu_x \Delta t + E - (-\bar{\mu}_x \Delta t + E) \\ &= (d\mu_x + \bar{\mu}_x) \Delta t \\ &= \mu_x \Delta t \\ \Delta x''_g &= \Delta' x_g - \Delta' x_g = 0 \end{aligned} \quad (6)$$

Once all of the plates have been reduced to one system, for every detected object a linear fit is applied to the corresponding transformed multi-epoch observations to obtain the absolute proper motions (and a reference position) as follows:

$$\begin{cases} x_t = x_0 + \mu_x(t - t_0) \\ y_t = y_0 + \mu_y(t - t_0) \end{cases} \quad (7)$$

⁴See subsection 3.3 for details on thresholds set for outlier rejection.

where x_t, y_t are the transformed plate (measured) coordinates at epoch t , and μ_x, μ_y, x_0, y_0 are the estimated absolute proper motions and positions in the same coordinate system at the chosen reference epoch $t_0 = J2000.0$ (see the paragraph on Step 7 in sec. 3.3). The x_0, y_0 are the positions at the reference epoch from all plates in different colors and epochs; this decreases the influence of individual random errors and improves the final precision.

3.2. Accurate orientation to the Equatorial system

The overall procedure just discussed only removes the systematic errors between reference and program plates; it can not remove the systematics inherent to the differences between plate-based coordinates and the standard coordinates.

This last registration is obtained using an external reference catalog and an account of the procedure follows.

We use a gnomonic projection to transform the estimated measured coordinates to an equatorial system. Since the Schmidt design provides an equidistant projection, we correct the measured coordinates following Dick (1991):

$$\begin{cases} x_G = x_0 + \frac{1}{3}x_0(x_0^2 + y_0^2) \\ y_G = y_0 + \frac{1}{3}y_0(x_0^2 + y_0^2) \end{cases} \quad (8)$$

where x_G, y_G are the measured coordinates in a gnomonic projection. By differentiating equation (8) as a function of time we find the corresponding relations for proper motions:

$$\begin{cases} \mu_{x_G} = \mu_x(1 + x_0^2 + \frac{1}{3}y_0^2) + \frac{2}{3}x_0y_0\mu_y \\ \mu_{y_G} = \mu_y(1 + y_0^2 + \frac{1}{3}x_0^2) + \frac{2}{3}x_0y_0\mu_x \end{cases} \quad (9)$$

where μ_{x_G}, μ_{y_G} are the proper motions in a gnomonic projection.

The transformation between the measured coordinates x_G, y_G and their celestial standard coordinate ξ, η can be expressed as

$$\begin{cases} \xi = ax_G + by_G + c + \varepsilon(x_G, y_G) \\ \eta = a'x_G + b'y_G + c' + \varepsilon'(x_G, y_G) \end{cases} \quad (10)$$

where a, b, c, a', b', c' are the coefficients of the linear terms of the plate model, i.e., axis direction, scale and origin difference between the measured

and standard coordinate systems; $\varepsilon(x_G, y_G)$ and $\varepsilon'(x_G, y_G)$ represent the higher order terms.

If we differentiate equation (10) with respect to time, we get the proper motions in the standard coordinate system.

$$\begin{cases} \mu_\xi = a\mu_{x_G} + b\mu_{y_G} \\ \mu_\eta = a'\mu_{x_G} + b'\mu_{y_G} \end{cases} \quad (11)$$

where we have neglected higher order terms, which we estimate to be less than 0.03% of the μ_x, μ_y .

For the objects on the plate, there is a precise geometrical relationship between the standard coordinates and equatorial coordinates i.e.

$$\begin{cases} \tan(\alpha - \alpha_0) = \frac{\xi}{\cos \delta_0 - \eta \sin \delta_0} \\ \tan(\delta) = \frac{\eta \cos \delta_0 + \sin \delta_0}{\cos \delta_0 - \eta \sin \delta_0} \cos(\alpha - \alpha_0) \end{cases} \quad (12)$$

where α_0, δ_0 are the equatorial coordinates of the tangent point.

Finally, the rigorous relationship between proper motions in the equatorial and standard systems is obtained by differentiating equation (12) as a function of time, i.e.

$$\begin{cases} \mu_\alpha = \cos^2(\alpha - \alpha_0) \left(\frac{1}{\cos \delta_0 - \eta \sin \delta_0} \mu_\xi + \frac{\xi \sin \delta_0}{(\cos \delta_0 - \eta \sin \delta_0)^2} \mu_\eta \right) \\ \mu_\delta = \cos^2(\delta) \left(\frac{\cos(\alpha - \alpha_0) \cos \delta_0}{\cos \delta_0 - \eta \sin \delta_0} \mu_\eta + \frac{\cos(\alpha - \alpha_0)(\eta \cos \delta_0 + \sin \delta_0) \sin \delta_0}{(\cos \delta_0 - \eta \sin \delta_0)^2} \mu_\eta - \frac{(\eta \cos \delta_0 + \sin \delta_0) \sin(\alpha - \alpha_0)}{\cos \delta_0 - \eta \sin \delta_0} \mu_\alpha \right) \end{cases} \quad (13)$$

3.3. Processing pipeline

We developed a FORTRAN pipeline based on the above principles to determine absolute proper motions from the COMPASS database. The flowchart (Fig.2) summarizes the specific steps and techniques used to remove the systematic errors and to acquire the absolute proper motions. Key steps in the flow chart are detailed below.

In **Steps 1 – 3** we extract all matches on the plates overlapping with the reference plate. Only objects that appear in all plates are used to calibrate the fit to the reference plate system.

In **Step 4**, a moving-mean-like method is applied to remove the mean shift (PdE and the mean

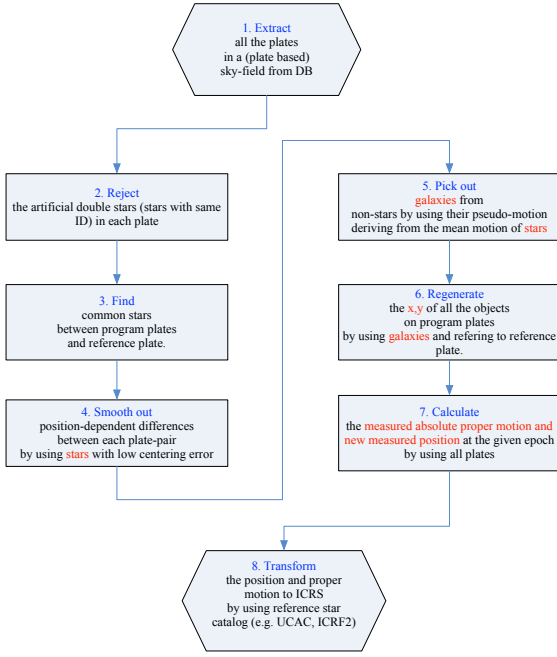


Fig. 2.— Flowchart of the processing pipeline

proper motions of reference stars) in x and y between the program and reference plate. Only stellar objects are used in the calculation of the moving mean but the result is applied to all detections. In order to attain the most accurate coordinate transformation, we select reference stars with good image quality, i.e., in the middle of the unsaturated magnitude range where the centering errors are minimized. In particular, we use detections classed as star in the range $(m_{\text{lim}} - 4.5) \leq m \leq (m_{\text{lim}} - 2.0)$, where m_{lim} is the limiting magnitude of the plate. In general we find around 500 stars degree $^{-2}$ well distributed on the plate. There are several methods for removing the PdE, such as a global plate solution using high-order polynomials, the astrometric MASK (Taff et al. 1990), the Infinitely Overlapping Circles (IOC, Taff et al. 1992), the sub-plate method (Taff 1989) etc. All these methods have pros and cons: the Schmidt plate distortions would require very complicated global solutions, the MASK method is very sensitive to the number of reference objects and the grid size, the IOC has problems at the plate boundaries and the sub-plate method can lead to non-uniformities.

We developed a variant of the sub-plate method, the Moving Sub-plate method, that is sensitive to

local signals while ensuring an increased level of uniformity. The Moving Sub-plate method starts by transforming the measured coordinates x_2, y_2 on the program plates to the corresponding coordinates x_1, y_1 on the reference plate using cubic polynomials (equation (14)). This will remove most of the large-scale errors (e.g. spherical deformation).

$$\begin{cases} x_1 = f(x_2, y_2) \\ y_1 = g(x_2, y_2) \end{cases} \quad (14)$$

where the functions f and g are complete cubic polynomials.

The residuals $\Delta x, \Delta y$, from the global (whole plate) cubic polynomial fit are then used in the following linear relations:

$$\begin{cases} \Delta x = ax_2 + by_2 + c \\ \Delta y = a'x_2 + b'y_2 + c' \end{cases} \quad (15)$$

where a, b, c, a', b', c' allow for zero point, rotation, and scale difference at a local level.

To fit equations (15) we select up to 15 nearby reference stars out to a maximum radius of 20 arcminutes from the program object. The size of the sub-plates automatically follow the reference star density. Applying this correction to all program objects removes most of the small scale errors (See Fig. 3). After Step 4, the mean displacement due to proper motion of the reference objects is locally zero, while that of galaxies is not.

In **Step 5** we use equation (16) on all the non-stars to fit a linear (coordinate only) model to estimate the mean proper motion components for any given plate pair, i.e., the $-\bar{\mu}_x \Delta t$ in equation 5, and its analogue for the y direction.

$$\begin{cases} \Delta x = x_1 - x_2 = ax_2 + by_2 + c \\ \Delta y = y_1 - y_2 = a'x_2 + b'y_2 + c' \end{cases} \quad (16)$$

here x_2, y_2 are intended as the measured coordinates of non-stars on the program plate corrected for the systematics calculated in Step 4. As per equation 5, we iterate rejecting any objects with residuals greater than 2.6 standard deviations per coordinate.

The objects that survive this selection are likely to be, or act like (i.e. non-stellar objects with zero proper motions), genuine galaxies. Fig. 4 shows the final mean (pseudo) proper motion of

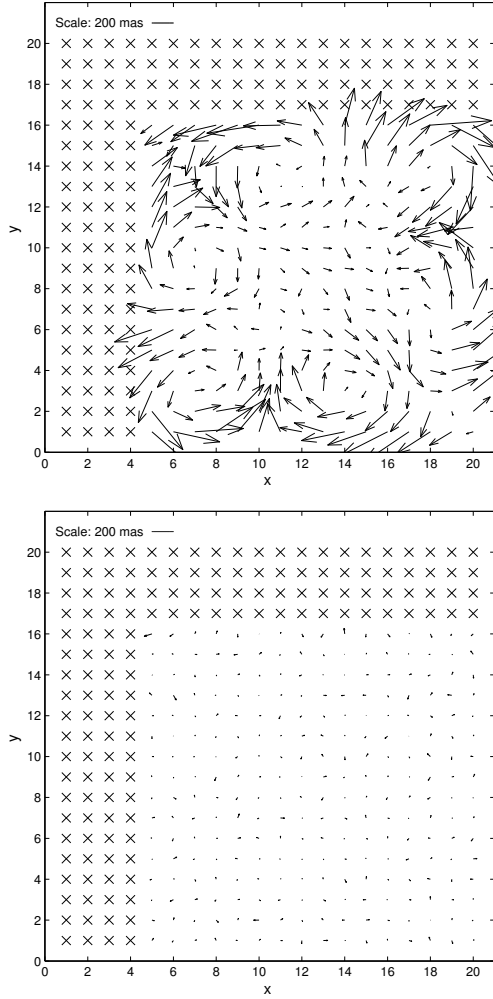


Fig. 3.— The upper figure shows the PdE as a function of plate position after the cubic polynomials fitting. The vector represents the magnitude and direction of the average residual for the reference stars in that region of the plate. The data shown here comes from the plate XP715 (epoch=1996.3, $l = 266.9^\circ, b = 69.2^\circ$) and XE494 (epoch=1955.3). The lower figure shows the same data as the one above after applying the Moving Sub-plate method. No observable PdE remains after this step. The marker ‘ \times ’ symbols indicate there are no common stars in those plate regions.

the galaxies after completing Step 5 for the same plate pair as that of Fig. 3.

In **Step 6** once the galaxies positions are corrected using the fitted coefficients of equation (16),

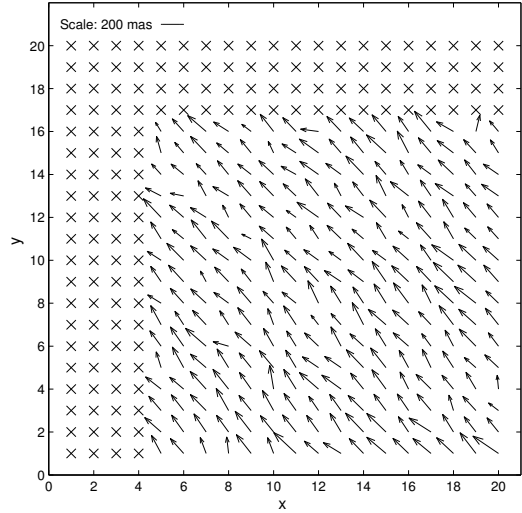


Fig. 4.— The mean pseudo ‘proper motion’ of galaxies as a function of plate position

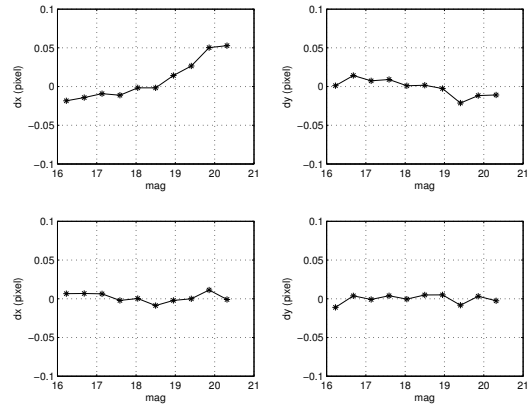


Fig. 5.— The mean residuals of the pseudo ‘proper motion’ of the galaxies as a function of magnitude after step 6. The upper two figures are the results without a magnitude term, while the lower panels are results with those terms.

a two-dimensional map of the galaxies residuals shows that some PdE are still present. These are smoothed out using again the moving sub-plate method but this time using the selected galaxies as reference objects. The residual corrections found at this stage are applied to all of the objects. The subset of these values relative to the galaxies is then spatially binned and plotted against magnitude and color to seek for any remaining MdE and/or CdE signals. In case, these are treated

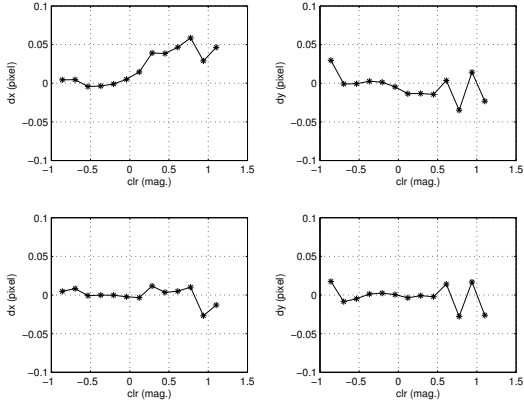


Fig. 6.— Shows the same residuals as Fig. 5, but as a function of color.

by simple one-dimensional linear interpolation in between the magnitude or color bins. This procedure removes most of the MdE and CdE between program and reference plates.

At this step we apply the mean motion to the stellar objects and remove it from the galaxies. From Figures 5 and 6 we note that both MdE and CdE were significantly reduced.

In **Step 7** for all of the plate objects we fit equation (7) to determine absolute proper motions and positions at the given epoch J2000.0. We then correct the measured coordinates and absolute proper motions derived in an equidistant projection to a gnomonic projection by using equations (8) and (9).

In **Step 8** we use the Fourth US Naval Observatory CCD Astrograph Catalog (UCAC4, Zacharias et al. 2013) and equations (10), (11), (12) and (13) to transfer absolute proper motions and positions to the celestial reference frame. Moreover, we corrected the frame bias between APOP and ICRS by using 1288 objects (most of them are faint Quasi-stellar objects) common to the radio ICRF2 catalog (Ma et al. 2009). To establish the orientation to the standard frame, we use the following formula

$$\begin{aligned} \vec{r}_{ICRF2} &= R_Y(\xi_y)R_X(\xi_x)R_Z(\xi_z) \cdot \vec{r}_{APOP} \\ &= \begin{pmatrix} 1 & \xi_z & -\xi_y \\ -\xi_z & 1 & \xi_x \\ \xi_y & -\xi_x & 1 \end{pmatrix} \cdot \vec{r}_{APOP} \end{aligned} \quad (17)$$

where \vec{r}_{ICRF2} and \vec{r}_{APOP} are the direction vectors to the common objects in both ICRF2 and APOP,

respectively; ξ_x, ξ_y, ξ_z are the three small rotation angles needed to register the APOP coordinate frame about the x, y and z axes of the ICRF2. A least-squares fit to equations (17) provides estimates of those three angles: $\xi_z = 27.73 \pm 0.12$ mas, $\xi_x = -7.30 \pm 0.15$ mas, and $\xi_y = 2.21 \pm 0.06$ mas; these are used to bring APOP onto ICRF2. After performing the transformation, the coordinate axes realized by our astrometric data are believed to be aligned with the extragalactic radio frame to within ± 0.2 mas at the reference epoch J2000.0.

4. CATALOG ACCURACY

We can estimate the accuracy and precision of our proper motions to provide us with a final external check. We expect the accuracy defined by the absolute zero point from equation (16), assuming the observational errors are equally distributed among the fitted parameters, to be approximately given by:

$$\sigma_{zero} = \frac{\sqrt{6}\sigma_g}{|\Delta t| \sqrt{N_g}} \quad (18)$$

where σ_g is the positional measuring error of galaxies, 6 is the number of unknown parameters and Δt is the epoch difference between two plates. This empirical error estimate has been confirmed by examining the formal error using simulated data. The range of positional measuring error of galaxies is in the range $0.^{\circ}2 < \sigma_g < 0.^{\circ}5$ for objects brighter than $R_F = 20.0$, the time baseline range is $12 < |\Delta t| < 45$ years and the number of galaxies is $8000 < N_g < 20000$. This corresponds to a zero-point (absolutization) error of $0.1 < \sigma_{zero} < 1.1$ mas/yr.

If we assume the observations are evenly distributed about the mid-epoch we find that the formal error of each proper motion component from equation (7) is

$$\sigma_\mu = \frac{\sigma_s}{\langle |\Delta t| \rangle \sqrt{N_{obs}}} \quad (19)$$

where σ_s is the positional error, N_{obs} is the number of observations of a star and $\langle |\Delta t| \rangle$ is the average time difference between the various observations and the mid-epoch. The range of positional measuring error is $\sim 0.^{\circ}2 < \sigma_g < 0.^{\circ}3$ for stars brighter than $R_F = 20.0$, the number of observations $3 < N_{obs} < 15$, and the average time

differences $12 < |\Delta t| < 45$ years. This corresponds to a range of overall error of $1 < \sigma_\mu < 14$ mas/yr.

We reduced all the plates with $|b| \geq 27^\circ$ and carried out an error analysis to certify the reliability of the calibration software and the quality of the final catalog, as described in the next sections.

4.1. Internal accuracy

For each object, we calculated positions and proper motions by fitting equation (7) utilizing all of the measurements from the different epochs and colors. This provides the formal errors of the calibrated parameters ($\mu_{\alpha*} = \mu_\alpha \times \cos(\delta)$, μ_δ , α , δ), and an internal check of the APOP quality.

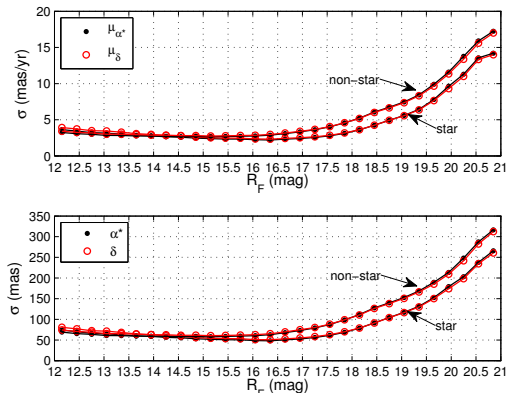


Fig. 7.— Mean formal errors of APOP absolute proper motions ($\mu_{\alpha*}, \mu_\delta$) and positions (α, δ) of stars and non-stars as a function of R_F magnitude. The magnitude is binned in 0.3 mag bins, with at least 100,000 objects per bin. The marker * in the μ_α indicates multiplication by $\cos(\delta)$. **Top:** the formal errors of absolute proper motions in mas/yr; **bottom:** the formal errors of positions in mas.

In Figure 7 we plot the mean formal errors and find them consistent in both right ascension and declination even though the two coordinates were treated independently. For stellar objects, the internal accuracy of the proper motions is better than ± 4 mas/yr for objects brighter than $R_F = 18.5$, increasing to 9 mas/yr at $R_F = 20.0$ and to 14 mas/yr for objects with $20.0 < R_F < 20.8$. The internal accuracy of the stellar positions is better than ± 100 mas for objects brighter than

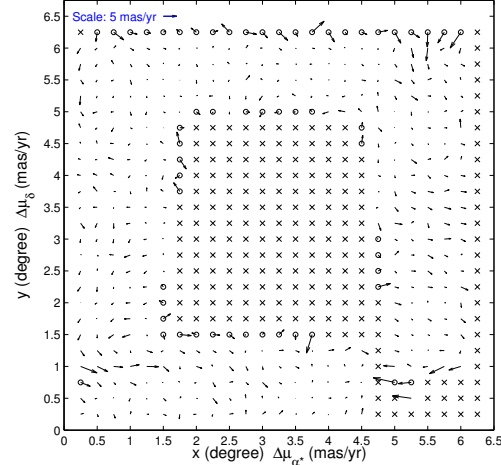


Fig. 8.— Differences of proper motions ($\Delta\mu_{\alpha*}, \Delta\mu_\delta$) of common objects in the reference plate XP216 and overlapping plates as a function of position. The ‘ \nearrow ’ indicates the magnitude and direction of the differences of the average proper motions. A 5 mas/yr scale arrow is plotted at the top left corner. The size of each bin is 0.25×0.25 degree 2 and they contain on average 300 objects per bin. The marker ‘ \times ’ indicates no objects in common, while a ‘ \circ ’ indicates that the number of the common objects is less than 100.

$R_F = 18.5$, increasing to 260 mas for objects with magnitude $R_F \sim 20.8$. The offset between the star and non-star objects is consistent with the ~ 1.5 times larger measurement errors of non-stellar objects.

We note that objects close to the magnitude limit (i.e $20 < R_F < 21$) have larger errors than predicted; APOP parameters and errors should be used with caution for objects fainter than $R_F = 20$.

An internal check of the accuracy of APOP proper motions is provided by multiple estimates for the same stellar objects appearing in overlap regions between adjacent reference plates. In Figure 8 we display the mean offset between the proper motions calibrated on two adjacent reference plates. The differences are plotted based on the position in the central reference XP216 ($l = 151.4^\circ, b = 62.8^\circ$) which has a typical $1.5^\circ \times 6.5^\circ$ overlap with four adjacent plates XP215 (left), XP217 (right), XP170 (top) and XP266 (bottom).

There are no large scale offsets in the overlap regions, but some shifts of ~ 1.8 mas/yr appear at small scales, particularly at the bottom left of the central plate. These are very likely caused by the uncertainty in the correction of the absolute zero point by the galaxies.

4.2. External accuracy

Quasi-stellar objects (QSOs) have star-like images and since they are extragalactic, they do not exhibit any time-dependent displacement. Thus, we can use the mean and dispersion of their measured motions to evaluate the zero point and overall precision of stellar proper motions. Here we use QSOs as an independent and direct determination of the APOP catalog quality.

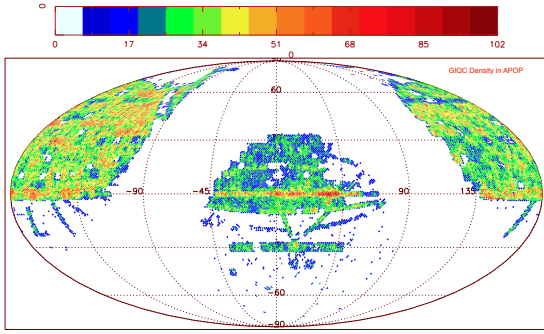


Fig. 9.— The density distribution of 376,490 QSOs found in the APOP catalog via cross-matching with the GIQC catalog.

The Gaia Initial QSO Catalog (GIQC) (Andrei et al. 2009) is chosen as the source list for known QSOs. The objects are broadly distributed within the SDSS region, though their density is not uniform (See Fig. 9). Figures 10, 11 and 12 show the mean proper motions of the GIQC QSOs and indicate that there is a very good agreement between the external and theoretical error estimates of proper motions for the magnitude range $R_F < 20.5$. In particular, from this sample of QSOs we find a proper motion zero point error of 0.6 mas/yr. As a verification of the internal estimates, Figure 13 shows the formal errors of positions (α, δ) of QSOs as a function of magnitude, and indicate that they are consistent with stellar objects.

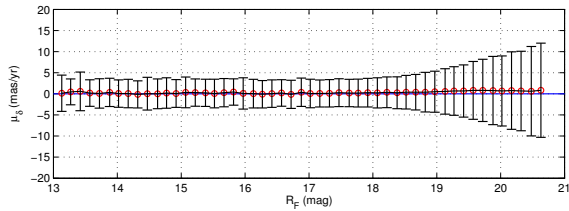
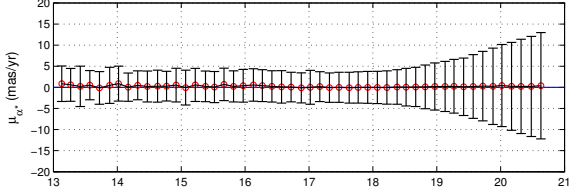


Fig. 10.— The distribution of absolute proper motions ($\mu_{\alpha*}$, μ_δ) of QSOs as a function of magnitude. The red circles indicate the mean of $\mu_{\alpha*}$ and μ_δ in that magnitude bin and the error-bar shows their standard deviation, which, following the assumption that QSO should have zero proper motions, are indicative of the proper motion random errors.

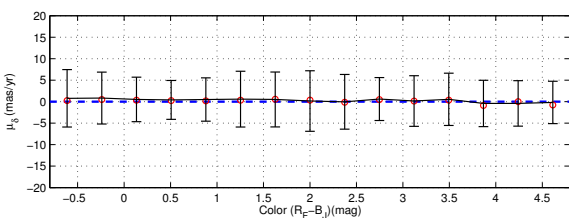
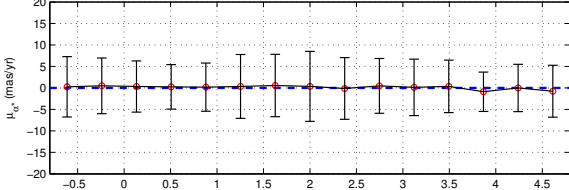


Fig. 11.— The absolute proper motions found for the QSOs as a function of color.

In addition to the GIQC, we also compared APOP with other external catalogs. The most natural comparison would be with the Positions and Proper Motion XL catalog (hereafter PPMXL, Roeser et al. 2010) the largest most recent catalog with absolute proper motions. This was constructed by combining USNO-B1.0 and the Two Micron All Sky Survey (Skrutskie et al. 2006) cat-

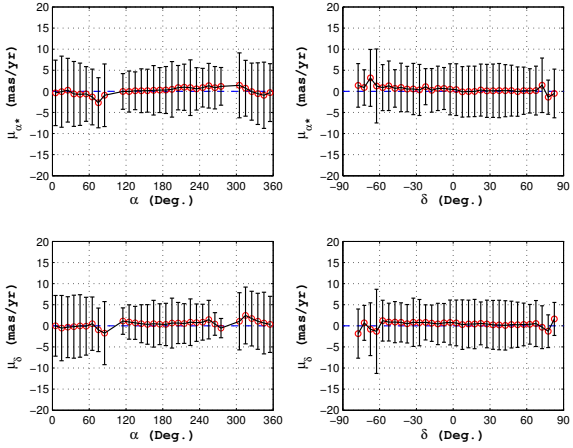


Fig. 12.— The absolute proper motions found for the QSOs as a function of α and δ .

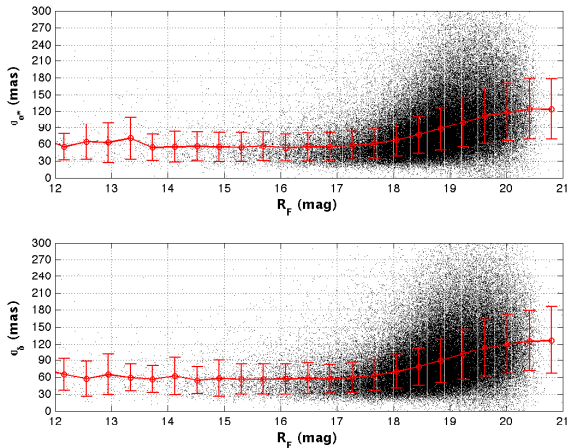


Fig. 13.— The formal errors of the QSO positions as a function of magnitude.

alogs. Figure 14 and 15 illustrate that there is a systematic offset between these two catalogs in absolute proper motions.

We also selected a subset of the GIQC QSOs that were in both the APOP and the PPMXL for a comparison. Figure 16 shows that the offset between the two catalogs is mostly due to a zero point problem in the PPMXL. Also for most of the magnitude range the APOP has smaller proper motion dispersion.

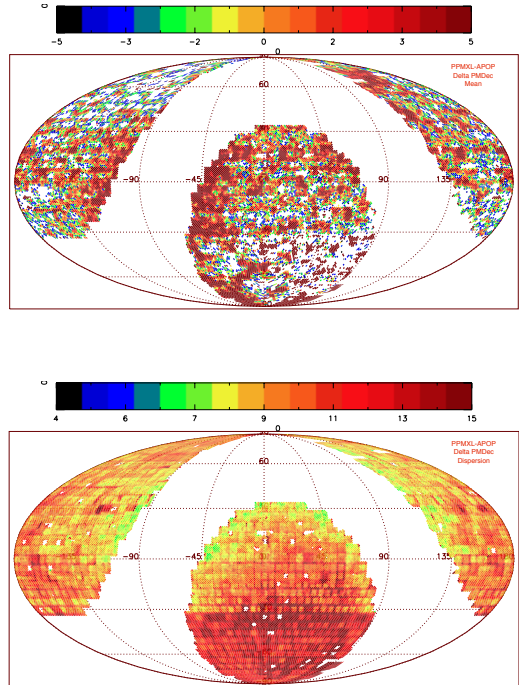


Fig. 14.— The mean (Top figure) and the dispersion (Bottom figure) of differences in μ_δ between APOP and PPMXL as a function of sky location in an equatorial coordinate system. The differences in μ_{α^*} are quite similar. These plots are based on the 82,722,482 common objects between these two catalogs divided in HEALPix (Hierarchical, Equal Area, and iso-latitude Pixelisation) level 6 regions.

4.3. Galactic clusters in APOP

Since the field of view of the Schmidt plate is very large (6.5×6.5 sq. deg) the mean proper motion of stellar objects could vary across the plate. For example, clusters generally cover a significant part of a photographic plate. Using the stars in Step 4 to remove the PdE we risk also “removing” the proper motions for this group of objects. Theoretically, we believe our procedure returns the mean proper motions to those groups with Steps 5 and 6. The proper motions of the Praesepe cluster in Figure 17 indicates that at least for this cluster the procedure has worked.

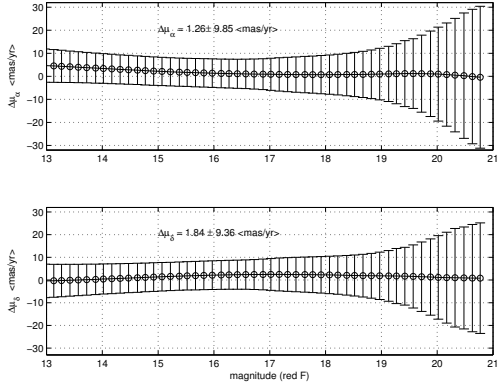


Fig. 15.— Mean and dispersion (RMS) of the proper motion differences between APOP and PPMXL as a function of magnitude.

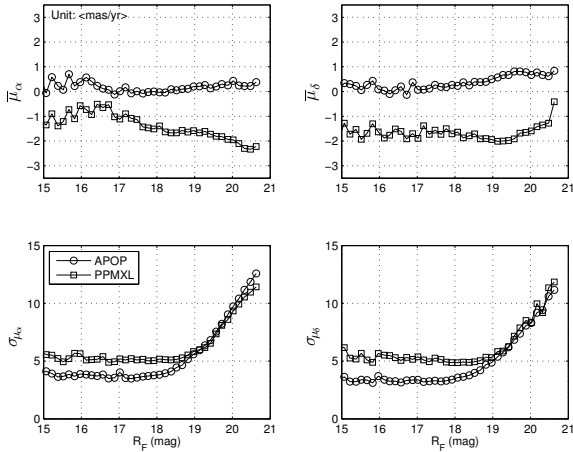


Fig. 16.— Mean and dispersion of the absolute proper motions of the 360,127 QSOs common to both the APOP and the PPMXL as a function of magnitude.

4.4. The final catalog

The catalog is available at Strasbourg's astronomical Data Center (<http://cds.u-strasbg.fr>); the description of the catalog data is detailed in Table 1.

Given the evidence provided, we believe that APOP's proper motions are reliable for operational applications as well as astrophysical research. However, the user should remember that the accuracy is best for objects with $\delta \geq -30^\circ$ because of the 45-year epoch difference between first and second generation survey plates; at lower

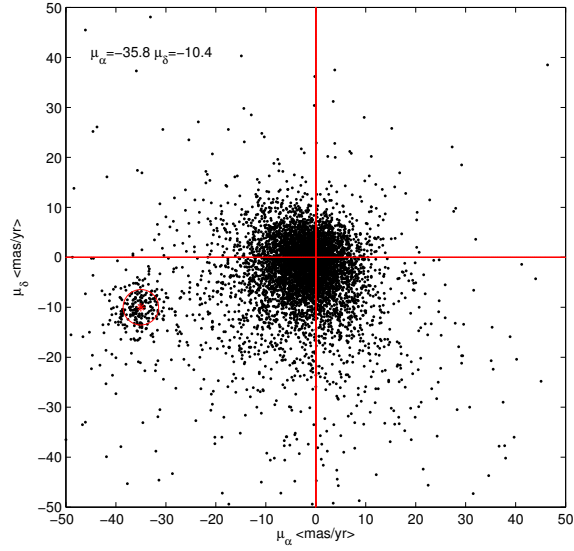


Fig. 17.— The proper motion vector-point diagram for all the objects in APOP with magnitude $R_F < 18.0$ in the area of the Praesepe cluster. A tight group at $\mu_{\alpha*} = -35.8 \text{ mas/yr}$, $\mu_{\delta} = -10.4 \text{ mas/yr}$ indicates the location of Praesepe and permits a segregation between the cluster and field stars. In addition, this value is quite close to the Hipparcos data for Praesepe, which is $\mu_{\alpha*} = -35.81 \text{ mas/yr}$, $\mu_{\delta} = -12.85 \text{ mas/yr}$ (van Leeuwen 2009).

declinations the quality can be about four times worse than that due to a time base of only 12 years.

Finally, the accuracy may not be sufficiently good for objects with magnitude $R_F < 15.0$ due to a lack of bright galaxies on some plates.

5. CONCLUSIONS AND FUTURE WORK

The main results from our study are:

- The principles and techniques suitable for the derivation of absolute proper motions from survey plates, including the treatment for position, magnitude and color systematics are described.
- The realization of the APOP catalog is presented. Because of the direct use of extragalactic objects, the catalog sky coverage is limited to the regions outside the galactic plane ($|b| \geq 27^\circ$).

Table 1: Description of the APOP data table.

number	Type	Units	Label	Explanations
1	Char	null	ID	source identifier ^a
2	Int	null	Type	Classification ^b
3	Double	degree	RA	α_{ICRS} , J2000.0
4	Double	degree	DE	δ_{ICRS} , J2000.0
5	Float	mas	sigRA	Error in α
6	Float	mas	sigDE	Error in δ
7	Float	mas/year	PR	$\mu_\alpha \cos(\delta)$
8	Float	mas/year	PD	μ_δ
9	Float	mas/year	sigPR	Error in $\mu_\alpha \cos(\delta)$
10	Float	mas/year	sigPD	Error in μ_δ
11	Int	null	Nobs	Number of observations ^c
12	Float	year	Dt	Maximal time differences ^d
13	Float	mag	Rmag	R_F photographic magnitude ^e
14	Float	mag	Bmag	B_J photographic magnitude
15	Float	mag	Nmag	I_N photographic magnitude
16	Float	mag	Vmag	V photographic magnitude
17	Float	mag	Jmag	2MASS J magnitude ^f
18	Float	mag	Hmag	2MASS H magnitude
19	Float	mag	Kmag	2MASS K_s magnitude

Note (a): The ID is the source identifier for object in the APOP, which is as same as the source identifier of that object in GSC2.3 catalog.

Note (b): The classification is based on the following codes:

0 : star as defined in the GSC2.3

1 : stars used as reference objects

2 : QSOs from the GIQC catalog

3 : nonstars as defined in the GSC2.3

4 : nonstars indicated as extragalactic objects from section 3.2 step 5

Note (c): The Nobs is the number of plates used for deriving the μ_α , μ_δ of that objects.

Note (d): The Dt is the maximal time differences between the plates used for the calculation.

Note (e): The magnitudes data are extracted directly from GSC2.3 catalog. Users can identify the exact meaning by looking at the ‘Table 3’ in GSC2.3 paper (Lasker et al. 2008).

Note (f): The photometric data are the near-infrared J (1.25 μm), H (1.65 μm), and K_s (2.16 μm) from the 2MASS catalog (Skrutskie et al. 2006).

The internal and external accuracies of this new catalog are consistent with expectations. The overall accuracy of the absolute proper motions is in the 3 to 9 mas/yr range, with an absolute zero point error estimated at better than 0.6 mas/yr; this proves the feasibility and reliability of the principles and methods adopted for its construction. The average position accuracy is about 150 mas (per coordinate) with a systematic deviation from the ICRS around 0.2 mas.

- A new method to refine source classification and select bona-fide galaxies by implementing the concept of induced pseudo-motion is presented.

We intend to apply a variant of this procedure to the whole of the GSC-II database to produce the GSC2.4. Some of the methods in this paper are only applicable in regions with significant

numbers of extragalactic objects; therefore, we are working on new procedures for the galactic plane. Another residual source for concern is the offset between the magnitude systems of stars and galaxies (Lasker et al. 2008). This reduces the effectiveness of removing the magnitude and color systematic errors by using galaxies.

Further investigations will clarify these issues as we prepare to extend APOP to the all sky with the production of GSC2.4.

6. ACKNOWLEDGMENTS

This work is a joint study of the Shanghai Astronomical Observatory (SHAO), the Osservatorio Astrofisico di Torino (OATo) and the Space Telescope Science Institute (STScI). We would like to express our thanks to many former and present members of the GSC project for their support and effort for this large project. The STScI is operated by the Association of Universities for Research in Astronomy, for the National Aeronautics and Space Administration under contract NAS5-26555. This work is supported by grants from the National Science Foundation of China (NSFC No. 10903022), the IPERCOOL FP7 International Research Staff Exchange Scheme (No. 247593), and the Italian Space Agency through contracts I/037/08/0 and I/058/10/0 (“The Italian Participation in the Gaia Mission”).

This research has made use of the MCS database server system, developed by Giorgio Calderone and Luciano Nicastro, operated at OATo and SHAO. Finally, we wish to thank the people who gave us their suggestions and assistance throughout the realization of APOP, and especially Ming Zhao, William F. van Altena, Ramachrisna Teixeira, Nadia Maigurova, Andrei A. Humberto, Ronald Drimmel, Leigh Smith and Zi Zhu.

REFERENCES

- Andrei, A. H., Souchay, J., Zacharias, N., et al. 2009, A&A, 505, 385
- Curir, A., Lattanzi, M. G., Spagna, A., et al. 2012, A&A, 545, A133
- Curir, A., Serra, A. L., Spagna, A., et al. 2014, ApJ, 784, L24

Dick, W. R. 1991, Astronomische Nachrichten, 312, 113

Evans, D. W. & Irwin, M. 1995, MNRAS, 277, 820

Kuimov, K. V., Sorokin, F. D., Kuz'Min, A. V., & Barusheva, N. T. 2000, Astronomy Reports, 44, 474

Lasker, B. M., Lattanzi, M. G., McLean, B. J., et al. 2008, AJ, 136, 735

Lasker, B. M., Sturch, C. R., McLean, B. J., et al. 1990, AJ, 99, 2019

Lattanzi, M. G. 2012, Mem. Soc. Astron. Italiana, 83, 1033

Ma, C., Arias, E. F., Bianco, G., et al. 2009, IERS Technical Note, 35, 1

Morrison, J. E., Smart, R. L., & Taff, L. G. 1998, MNRAS, 296, 66

Roeser, S., Demleitner, M., & Schilbach, E. 2010, AJ, 139, 2440

Skrutskie, M. F., Cutri, R. M., Stiening, R., et al. 2006, AJ, 131, 1163

Spagna, A., Lattanzi, M. G., Lasker, B. M., et al. 1996, A&A, 311, 758

Spagna, A., Lattanzi, M. G., McLean, B., et al. 2004, MSAIt Supplement, 5, 97

Spagna, A., Lattanzi, M. G., Re Fiorentin, P., & Smart, R. L. 2010, A&A, 510, L4

Taff, L. G. 1989, AJ, 98, 1912

Taff, L. G., Bucciarelli, B., & Lattanzi, M. G. 1992, ApJ, 392, 746

Taff, L. G., Lattanzi, M. G., Bucciarelli, B., et al. 1990, ApJ, 353, L45

Tang, Z. H., Qi, Z. X., Yu, Y., et al. 2008, in IAU Symposium, Vol. 248, IAU Symposium, 334–336

van Leeuwen, F. 2009, A&A, 497, 209

Zacharias, N., Finch, C. T., Girard, T. M., et al. 2013, AJ, 145, 44

This 2-column preprint was prepared with the AAS **LaTeX** macros v5.2.